Journal of Fluorescence, Vol. 2, No. 1, 1992

Diffusion-Influenced Fluorescence Quenching Dynamics in One to Three Dimensions

Bo Medhage[1] and Mats Almgren[1,2]

Received February 12, 1992; revised May 6, 1992; accepted May 7, 1992

The fluorescence decay curves obtained from diffusion-influenced quenching in various spatial dimensions are discussed. The two-dimensional quenching has, because of intractable fitting functions, previously been dealt with only in the completely diffusion-controlled case (corresponding to the Smoluchowski boundary condition). In this paper, an approximation for the two-dimensional (2D)-quenching behavior with the Collins–Kimball boundary condition is presented. The nonlinear least-squares method has been used to analyze simulated decay data. The consequences the choice of an incorrect model has on the final results as well as the possibility to discriminate between different dimensionalities are investigated. Also, some inherent properties of the fitting functions are studied.

KEY WORDS: Fluorescence; quenching; diffusion; dimensionality.

INTRODUCTION

Fluorescence quenching, or the deactivation of excited species in general, often occurs on the first encounter of the excited species with the quencher and is then a diffusion-controlled process. The most familiar way to treat the dynamics of such processes has its origins in the work of Smoluchowski [1] and was recently analyzed and rederived in a clear and instructive way by Szabo [2], showing the limitations and the strengths of the approach. Expressions for the time-dependent rate constant of fluorescence quenching were presented, valid for different dimensions and both for the strictly diffusion controlled case and for the case that the reaction rate at encounter is finite, the so-called radiation or Collins–Kimball [3] boundary condition. The fluorescence decays after excitation with an infinitely narrow pulse can be calculated from these expressions and are presented below.

The application of these results to experimental studies of (quasi) one-dimensional (1D) [4,5] or three-dimensional (3D) systems presents no special problems; the two-dimensional (2D) case, however, is very difficult to handle numerically. The experimental studies of fluorescence quenching in quasi two-dimensional systems have always assumed complete diffusion control, since for this case an approximate solution due to Owen [6] has been available for the evaluation of the results. This approximation, however, is valid only over a limited time range and is, furthermore, somewhat in error numerically.

The two-dimensional case is of considerable importance; it is the case that would apply for diffusional quenching in monolayers [7], in bilayer membranes of vesicles and biological structures [8–10], and in lamellar surfactant phases [5,11]. All these systems are of course in reality three-dimensional, but as long as the thickness of the layer in which the probe and the quencher are moving is small compared to the lateral diffusive dis-

[1] Department of Physical Chemistry, Uppsala University, Box 532, S-751 21 Uppsala, Sweden.
[2] To whom correspondence should be addressed.

1053-0509/92/0300-0007$06.50/0

placement during the time of measurement, the 2D model is appropriate. The Smoluchowski boundary condition, assuming instant reaction at a certain lateral distance between the reactants, will normally not apply, however, not even for purely diffusion-controlled reactions, since the distance between the reactants also depends on their separation in the third dimension. This can be taken care of by assuming that the reaction occurs at a finite rate when the reactants are within a cylindrical reaction zone [4,5] with radius equal to the half-thickness of the layer in which the reactants are mobile; the Collins–Kimball boundary condition then has to be used. For the case where the probe and the quencher both are present in the same position in the third dimension (e.g., when they are both solubilized in the headgroup region of a surfactant), the reaction is probably still diffusion controlled.

Another interesting case, which has not yet been studied, and where the 2D model also should be applicable, is that of quenching on the surface of small micelles, when the fluorophore is so short-lived that many quenchers are required for an appreciable effect. The time window of the measurement is then so short that the reactants will not explore the full surface of the micelle. The fluorescence lifetime of the unquenched probe should be only a few nanoseconds at most.

In this paper, an approximate expression for the fluorescence decay in the 2D case with the Collins–Kimball boundary condition is presented, in a form suitable for implementation in computers for fitting to experimental data. The approximation for the 2D case and the expressions for the decays in the 1D and 3D cases are tested by extensive curve-fitting against simulated data in order to find how well the model parameters may be recovered and if discrimination between different models can be made.

A close examination of the chi-square hypersurface, associated with the fitting of diffusion-influenced fluorescence quenching data, is used to illuminate some inherent difficulties in the decay data analysis. Some general hints concerning both the designing and the analysis of diffusion experiments are given.

THEORY

The Smoluchowski Approach. In our formal treatment of the diffusive dynamics we follow the classical Smoluchowski approach [1] using the unified and comprehensive formalism presented by Szabo [2]. The crucial approximation in this treatment is that the excited probes (P*) are regarded as being stationary, while the quenchers (Q) are allowed to diffuse around them with the relative diffusion coefficient $D = D_{P^*} + D_Q$. This is correct when just one probe–quencher pair is considered, but it is not rigorously true when more than one quencher is present, since then the motion of the quenchers is not necessarily uncorrelated. However, in the many-particle formulation the Smoluchowski approach is exact in the limit when the diffusion coefficient of the probe approaches zero and the quenchers do not interact with each other, or when the quencher concentration is very low, so that only probe–quencher pairs are considered. Nevertheless, the Smoluchowski treatment is a very good approximation for solitary excited states surrounded by not too many noninteracting quenchers.

The fluorescence decay following a delta pulse excitation is given by

$$\ln\frac{F(t)}{F(0)} = -k_0 t - c_q \int_0^t k(t')dt' \qquad (1)$$

where k_0 is the natural decay constant, c_q the quencher concentration, and $k(t)$ the time-dependent second-order quenching rate constant, which is calculated from the time-dependent radial distribution function $p(r,t)$ of quenchers around the excited probe molecule.

In the Smoluchowski approach the probe P* is placed at the origin of a coordinate system and $p(r,t)$ is assumed to satisfy the diffusion equation in d dimensions,

$$\frac{\partial p(r,t)}{\partial t} = \frac{D}{r^{d-1}}\frac{\partial}{\partial r}\left(r^{d-1}\frac{\partial p(r,t)}{\partial r}\right) \qquad (2)$$

This equation can be solved subject to the initial condition

$$p(r,0) = 1 \qquad (3)$$

and the boundary condition

$$p(\infty,t) = 1 \qquad (4)$$

For the completely diffusion-controlled case, which implies infinite rate of reaction at the encounter distance a, Eq. (2) is solved subject to the Smoluchowski boundary condition

$$p(a,t) = 0 \qquad (5)$$

The resulting rate constant is denoted by $k_S(t)$ in the following.

With a finite rate of reaction on encounter, the radiation boundary condition of Collins and Kimball [3] applies:

$$\left(\frac{dp}{dr}\right)_{r=a} = hp(a,t) \qquad (6)$$

with

$$h = \frac{k_q a}{dD} \tag{7}$$

where k_q is a first-order quenching rate constant for the P*–Q pair in contact; h is thus a parameter that weights reaction against diffusion. Quite often a second-order rate constant $k(0)$ is used in the equivalent of Eq. (6), which is the initial value of the time-dependent quenching constant. We have the relationship

$$k_q = k(0)/V_a \tag{8}$$

The reason for using k_q originates from the reaction-zone concept, suitable for the consideration of quasi one- and two-dimensional systems. The probe molecule is thought to be surrounded by a cylindrical reaction zone of volume V_a, in which quenching takes place with the first-order rate constant k_q; the parameter a is then the radius of the cylinder or the half-thickness of the layer [4,5].

The time-dependent rate constant calculated from the radiation boundary condition is denoted $k_{CK}(t)$ and can be expressed [2] in terms of $k_S(t)$ as

$$\hat{k}_{CK}(z) = \frac{k_q V_a \hat{k}_S(z)}{k_q V_a + z\hat{k}_S(z)} \tag{9}$$

where $\hat{k}(z)$ is the Laplace transform of the rate constant $k(t)$ using the notation

$$\hat{k}(z) = \int_0^\infty e^{-tz} k(t)dt \tag{10}$$

It can be shown [2] that from the solution of the Laplace transform of Eq. (2), we get

$$\hat{k}_S(z) = \frac{2\pi^{d/2} D a^{d-2} x K_{d/2}(x)}{z\Gamma(d/2)K_{d/2-1}(x)} \tag{11}$$

where $x = (za^2/D)^{1/2}$, K_ν is the modified Bessel function of the second kind of order ν, and $\Gamma(d/2)$ is the gamma function. When the radiation boundary condition is used, $\hat{k}_{CK}(z)$ can be obtained from $\hat{k}_S(z)$ by using Eq. (9).

For the fluorescence decay, we are interested in the time integral of the rate constant, the Laplace transform of which is given by

$$\hat{I}(z) = \hat{k}(z)/z \tag{12}$$

From these equations the fluorescence decay functions are obtained via inverse Laplace transformation; the resulting expressions for 1D [4], 2D [12,13], and 3D [3] systems are given in the following section.

Fluorescence Decay Equations. A general description of a fluorescence decay curve in dimensionality d ($d = 1$, 2, or 3) is given by

$$\ln\frac{F(t)}{F(0)} = -k_0 t - a^3 c_q Q_d(ha, t/\tau_q) \tag{13}$$

with

$$Q_1(ha, t/\tau_q) = \frac{4\pi}{ha}\left\{\sqrt{\left(\frac{ha}{\sqrt{\tau_q}}\right)^2 \frac{t}{\pi}} + \frac{3}{4}\left[\exp\left\{\left(\frac{ha}{\sqrt{\tau_q}}\right)^2 \frac{4t}{9}\right\}\operatorname{erfc}\left\{\left(\frac{ha}{\sqrt{\tau_q}}\right)\sqrt{\frac{4t}{9}}\right\} - 1\right]\right\} \tag{14}$$

$$Q_2(ha, t/\tau_q) = \frac{16}{\pi}(ha)^2 \int_0^\infty \frac{1 - \exp\left(-\frac{t}{\tau_q}x^2\right)}{[xJ_1(x) + haJ_0(x)]^2 + [xY_1(x) + haY_0(x)]^2}\frac{dx}{x^3} \tag{15}$$

$$Q_3(ha, t/\tau_q) = \frac{4\pi ha}{\beta}\left\{\frac{t}{\tau_q} + \frac{ha}{\beta^2}\left[\exp\left\{\beta^2\frac{t}{\tau_q}\right\}\operatorname{erfc}\left\{\beta\sqrt{\frac{t}{\tau_q}}\right\} - 1\right] + \frac{2ha}{\beta}\sqrt{\frac{t}{\pi\tau_q}}\right\} \tag{16}$$

where $\tau_q = a^2/D$ and $\beta = 1 + ha$. $J_n(x)$ and $Y_n(x)$ are the Bessel functions of the first and second kind, respectively, of order n. The natural decay rate constant, k_0, is determined in a separate experiment and should thereafter be kept fixed in the analysis. The cylinder radius a (for 1D and 2D quenching) is assumed equal to the encounter radius. However, if the encounter radius, in the 2D case, is large (approximately greater than or equal to the layer thickness), the factor $a^3 c_q$ in Eq. (13) should be replaced by $za^2 c_q$, where z is the half-thickness of the layer. Note that for the 1D case, there are only *two* independent parameters (a^3/ha and $ha/\sqrt{\tau_q}$), while in the other two cases there are *three*. This implies that in the studies of one-dimensional diffusion, at least one parameter, usually the radius a, must be known (or guessed). Q_1 and Q_3 are, although complex, yet well-behaved and easily evaluated functions, whereas Q_2 is an extremely ill-behaved function. Due to the intractable integral expression in Q_2, two-dimensional diffusion has not been studied in any great detail except for the completely diffusion-controlled case (i.e., corresponding to the Smoluchowski boundary condition) [5–11], in which Q_2 reduces to

$$Q_{2,\infty} = Q_2(ha = \infty, t/\tau_q) = \frac{16}{\pi}\int_0^\infty \frac{1 - \exp(-\frac{t}{\tau_q}x^2)}{J_0^2(x) + Y_0^2(x)}\frac{dx}{x^3} \quad (17)$$

Owen [6] presented an approximation to this integral based on the functional form of the corresponding equation in three dimensions,

$$Q_{3,\infty} = Q_3(ha = \infty, t/\tau_q) = 8\sqrt{\pi}\sqrt{t/\tau_q} + 4\pi t/\tau_q \quad (18)$$

Assuming the same $8\sqrt{\pi}\sqrt{t/\tau_q}$ dependence as t approaches zero and choosing the linear term coefficient to give the best description of $Q_{2,\infty}$ in the range $0 \le t \le 10\tau_q$, Owen obtained

$$Q'_{2,\infty} = 14.180\sqrt{t/\tau_q} + 3.17t/\tau_q \quad (19)$$

However, due to the unfortunate intractability of the Q_2 integrals, Owen's numerical evaluation of Eq. (17) is slightly erroneous and underestimates the real value of $Q_{2,\infty}$ by more than 10% when $t/\tau_q \ge 1$.

A remarkable approximation for the corresponding time-dependent rate constant, $k_S(t)$, was presented by Szabo [2]. This approximation gives correctly the first two terms of both the short-time and the long-time expansions of the rate constant and reproduces its values within 1.3% at all times. By integrating the rate constant, we obtain

$$Q''_{2,\infty} = \frac{2}{D\tau_q}\int_0^t k_S(t')dt' = 4\pi\int_0^{t/\tau_q}\left(\frac{\exp(-\sqrt{\pi x}/10)}{\sqrt{\pi x}} + \frac{1}{\ln\{\sqrt{4e^{-\gamma}x} + e^{5/3}\}}\right)dx \quad (20)$$

where $\gamma = 0.5772156...$ (Euler's constant). This integral is easily evaluated numerically without large CPU-time consumption and is, therefore, a very suitable fitting function in the analysis of data for the purely diffusion-controlled case.

Evaluation of Q_2. The numerical evaluation of the function $Q_2(ha, t/\tau_q)$ is not straightforward. It must be evaluated with great care and precaution due to the intractable short-time behavior of the integrand. Some technical aspects on the evaluation of the Q_2 integral are presented, of main interest for those who want to use it directly in the analysis or create their own approximations. The problem can be treated in a semianalytical way by splitting the Q_2 function into three terms and using asymptotic expansions of the Bessel functions in both the short- and the long-time region, respectively. By substituting the Bessel functions with their asymptotic expansions, neglecting high-order terms and working out the integrals, we thus obtain the short-time term

$$Q_2^0 = 8\frac{t}{\tau_q}\left[\arctan\left(\frac{2}{\pi}\left[\ln\left(\frac{\epsilon}{2}\right) + \gamma - \frac{1}{ha}\right]\right) + \frac{\pi}{2}\right] \quad (21)$$

where ϵ (see below) is typically less than 10^{-4}, and the long-time term

$$Q_2^\infty = 8\left[\frac{1}{b} + \frac{1}{ha}\arctan\frac{b}{ha} - \frac{\pi}{2ha}\right] - 8(ha)^2\int_b^\infty \frac{\exp(-(t/\tau_q)x^2)\,dx}{x^2(x^2 + (ha)^2)} \quad (22)$$

where $b \ge 10$. The integral term in Q_2^∞ is easily and safely calculated numerically. The desired function is

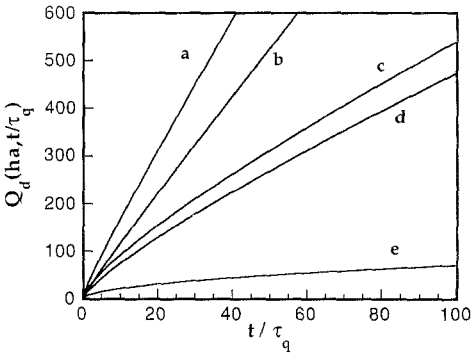

Fig. 1. $Q_d(ha, t/\tau_q)$ vs. dimensionless time, t/τ_q, for some values of ha. (a, b) Q_3 for $ha = \infty$, 3; (c, d) Q_2 for $ha = \infty$, 3; (e) Q_1 for $ha = \infty$; on this time scale $Q_1(ha = 3)$ is not much different from $Q_1(ha = \infty)$ and is, therefore, for the sake of clarity, not shown.

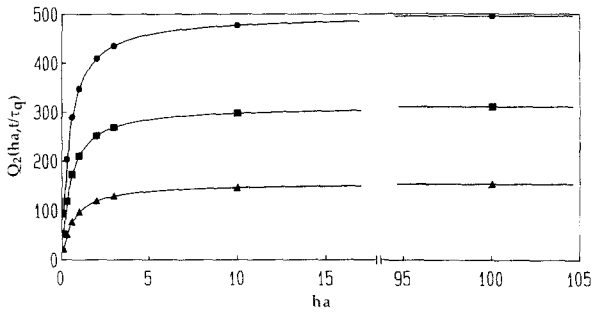

Fig. 2. Q_2 as a function of ha for three values of t/τ_q; from above, t/τ_q = 90, 50, 20. The solid lines represent fits to the data points according to Eq. (28) in the text. From the analysis the parameters $R(t/\tau_q)$ and $S(t/\tau_q)$ are obtained.

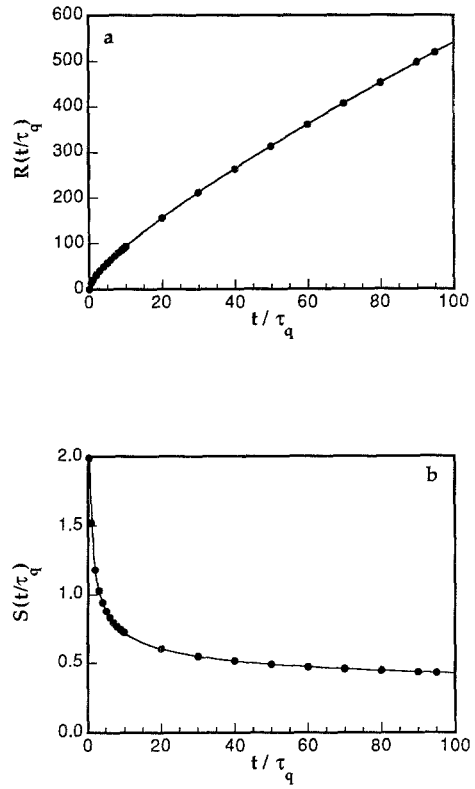

Fig. 3. The two parameters R and S vs. t/τ_q. Equations (29) and (30) have been used to extract the desired constants α and β and the $A_i : s$ as described in the text.

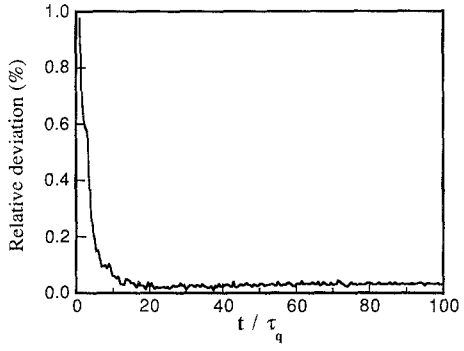

Fig. 4. The relative deviation, $(Q_2^{app} - Q_2^{true})/Q_2^{true}$, of the approximate Q_2 values [Eq. (31)] from the "true" ones [calculated using Eq. (15)] in the interval $t/\tau_q \in [1,100]$ for $ha = 7$. The value $ha = 7$ was chosen, as it was not used in the determination of the constants in Eq. (31).

thus given by

$$Q_2(ha, t/\tau_q) \simeq Q_2^0 + Q_2^{num} + Q_2^\infty \qquad (23)$$

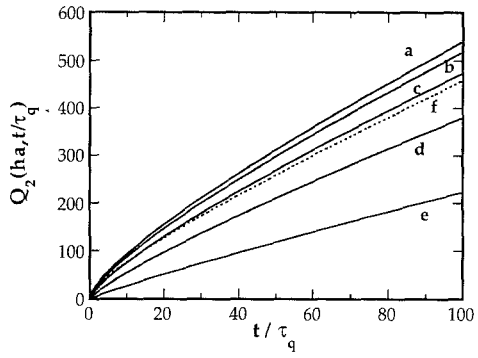

Fig. 5. Q_2 as a function of t/τ_q for some values of ha: (a) Q_2 ($ha = \infty$); (b) Q_2 ($ha = 10$); (c) Q_2 ($ha = 3$); (d) Q_2 ($ha = 1$); (e) Q_2 ($ha = 0.3$); (f) Owen's approximation from Eq. (19).

The intermediate function

$$Q_2^{num} = \frac{16}{\pi}(ha)^2 \int_\epsilon^b \frac{1 - \exp(-(t/\tau_q)x^2)}{[xJ_1(x) + haJ_0(x)]^2 + [xY_1(x) + haY_0(x)]^2} \frac{dx}{x^3} \qquad (24)$$

remains to integrate numerically but is much easier to evaluate than the corresponding improper integral [Eq. (15)]. We strongly recommend that this integral is split up in several subintegrals to improve the accuracy of the calculation further.

For purely diffusion-controlled quenching the functions equivalent to Eqs. (21) and (22) are

$$Q_{2,\infty}^0 = 8\frac{t}{\tau_q}\left[\arctan\left(\frac{2}{\pi}\left[\ln\left(\frac{\epsilon}{2}\right) + \gamma\right]\right) + \frac{\pi}{2}\right] \qquad (25)$$

and

$$Q_{2,\infty}^\infty = 8\left[\frac{1 - \exp(-(t/\tau_q)b^2)}{b} + \sqrt{\pi}\sqrt{t/\tau_q}\,\mathrm{erfc}(b\sqrt{t/\tau_q})\right] \qquad (26)$$

It is interesting to note that the expected $8\sqrt{\pi}\sqrt{t/\tau_q}$ behavior is obtained in the short-time domain, in which both $Q_{2,\infty}^0$ and $Q_{2,\infty}^{num}$ are vanishingly small as compared to $Q_{2,\infty}^\infty$. It should also be pointed out that numerical calculations show that in the long-time region, the intermediate term $Q_{2,\infty}^{num}$ can never be neglected as compared to the linear term $Q_{2,\infty}^0$. In other words, Q_2 will never exhibit a linear t/τ_q dependence as implied by Owen's approximation. Figure 1 shows Q_d as a function of t/τ_q at two values of ha ($= 3,\infty$) for one-, two-, and three-dimensional quenching.

Simulation of Fluorescence Decay Data. Time-cor-

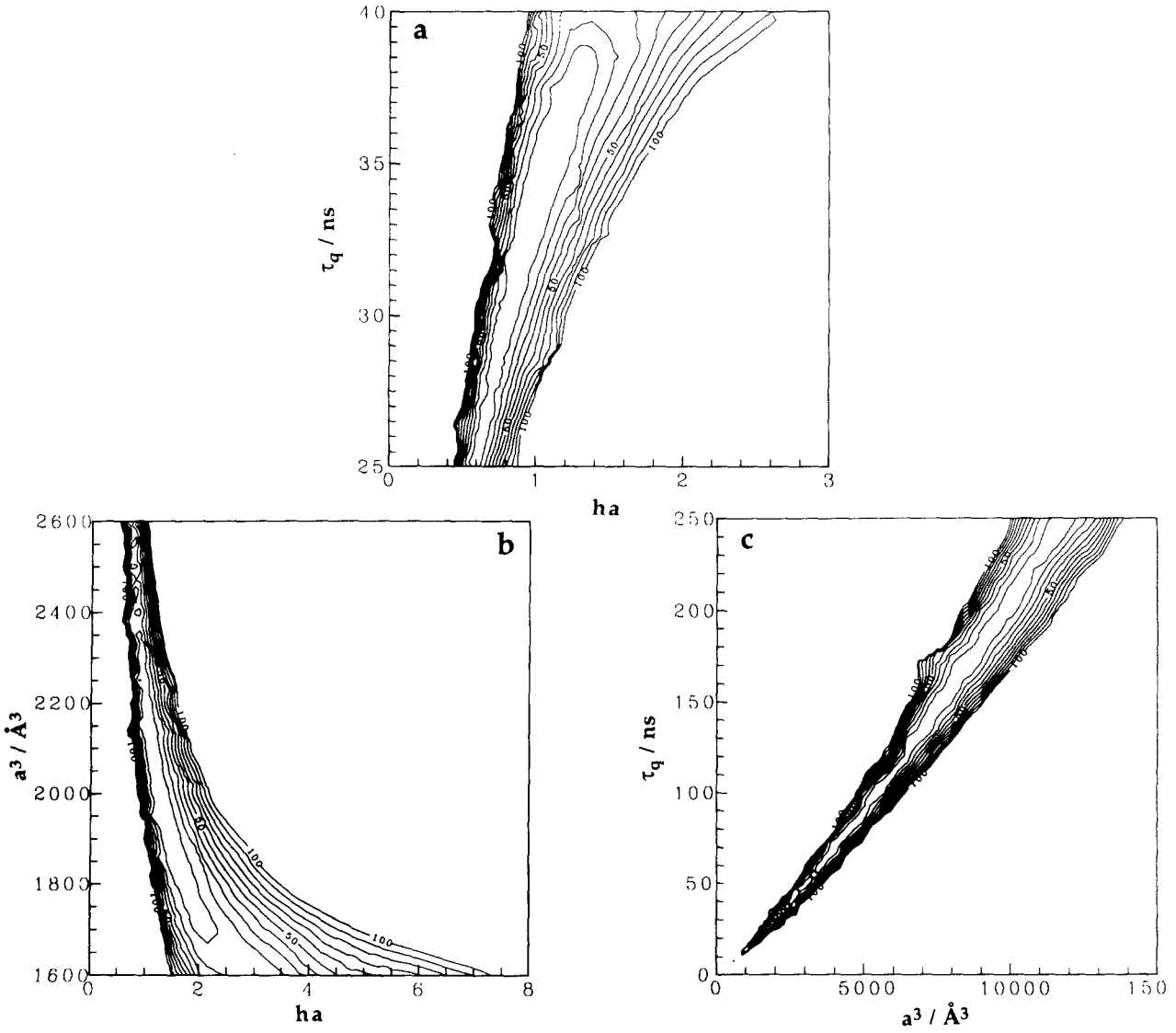

Fig. 6. Contour plots of cross sections of the 2D quenching chi-square hypersurface $\chi^2 = f(ha, \tau_q, a^3)$, where the global minimum is located at $(ha, \tau_q, a^3) = (1, 33.8, 2197)$. The contour levels shown correspond to $\chi^2 \leq 100$ with $\Delta\chi^2 = 10$: (a) $\chi^2 = f(ha, \tau_q)$; (b) $\chi^2 = f(ha, a^3)$; (c) $\chi^2 = f(a^3, \tau_q)$.

related single photon counting data were synthesized according to Eqs. (14) and (16) [in combination with Eq. (13)] for the 1D and 3D cases, respectively, and the method outlined above [Eqs. (21) to (24)] was used for the 2D case. A useful long-time approximation of $\exp(x^2)\mathrm{erfc}(x)$ [14] in the simulations of 1D and 3D decay curves is

$$\exp(x^2)\mathrm{erfc}(x) \simeq \frac{1}{x\sqrt{\pi}} \tag{27}$$

The numerical evaluation of the Q_2 integral was performed by Romberg integration.

Gaussian noise of zero mean and variance equal to the number of counts was added to channels with more than 20 counts. For channels with less than 20 counts a Poissonian noise generator was used.

Fluorescence Data Analysis. The fluorescence decay data were analyzed with the nonlinear least-squares (NLLS) technique using a modified Levenberg–Marquardt algorithm [15], which eliminates the need for explicit partial derivatives.

The reduced χ^2 value was used to judge the quality of the fit.

Table I. Numerical Values of the Empirical Constants in the Approximation of the Function $Q_2(ha,t/\tau_q)$[a]

t/τ_q-interval	Parameter value					
	α	β	A_1	A_2	A_3	A_4
[100,1000]	0.90471	−0.097394	6.26616	13.7204	0.50665	1.00797
[1,100]	0.90281	−0.080878	6.37002	13.4052	0.46560	1.05439
[0.1,1]	0.96902	−0.201078	5.37842	14.4301	0.57118	0.94262
[0.01,0.1]	0.92521	0.12850	5.36093	14.2470	0.84851	1.04004
$[10^{-3},0.01]$	1.88892	−1.2259	125.929	14.7764	2.12×10^{-4}	1.06576
$[10^{-5},10^{-3}]$	0.48612	−0.50815	7.26816	6.84802	1.95887	−0.96553

[a] A description of how the constants have been determined is given in the text.

Table II. Illustration of How the Maximum Value of the Function $(\Delta F/\sqrt{F})(t)$ Depends on the Relative Error in the Approximation of Q and on the Quencher Concentration[a]

a^3c_q	$\lvert\Delta Q/Q\rvert$	$(\Delta F/\sqrt{F})_{max}$
0.022	0.001	0.108
	0.005	0.542
	0.010	1.084
	0.10	10.8
	0.15	16.2
0.22	0.001	0.161
	0.005	0.804
	0.010	1.607
	0.10	16.1
	0.15	24.1

[a] The other parameters were $F(0) = 50000$, $ha = 10$, $\tau_q = 35$ ns, and $\tau_0 = 300$ ns.

RESULTS AND DISCUSSION

Creation of an Approximation to $Q_2(ha, t/\tau_q)$. To use Eqs. (21) to (24) directly in the analysis proved to be unfeasible due to the large amount of computational time required to calculate the integrals numerically with sufficient precision. The NLLS method is well-known to be rather sensitive to the initial estimates of the fitting parameters; badly chosen starting values often lead to overflow errors in the programs or cause the analysis to end up in a *local* minimum (sometimes, but not always, indicated by a poor χ^2 value) instead of in the *global* one. Multiple sets of initial guesses should be used, therefore, to ensure that a global minimum is found and to check the dependence of the results on the starting values. This kind of tests makes the analysis even more CPU time-consuming and the necessity for a more practicable way of analysis is evident.

To make the fitting function more tractable we have created an approximation to Eq. (15) following the procedure described below. Q_2 was calculated for a large set of ha and t/τ_q values. For each t/τ_q, the dependence of Q_2 on ha, as exemplified in Fig. 2, was described by the function

$$Q_2 = \frac{R\,ha}{S + ha} \tag{28}$$

and the parameters R and S were determined by fitting this equation to each data set. The dependence of R and S on t/τ_q could be well described by Eqs. (29) and (30), respectively (Fig. 3), for limited ranges of t/τ_q values. (The reason for dividing the t/τ_q values into several intervals was to produce an equally good description of the Q_2 function at all times t/τ_q.)

$$R = A_1(t/\tau_q)^{\alpha} + A_2\sqrt{t/\tau_q} \tag{29}$$

$$S = A_3(t/\tau_q)^{\beta} + A_4\sqrt{t/\tau_q} \tag{30}$$

The parameters α, β, and A_1–A_4 were determined for six ranges of t/τ_q values with results as shown in Table I.

By combining Eqs. (28), (29), and (30) the approximation for Q_2 is obtained as

$$Q_2^*(ha, t/\tau_q) = \frac{[A_1(t/\tau_q)^{\alpha} + A_2\sqrt{t/\tau_q}]ha}{A_3(t/\tau_q)^{\beta} + A_4/\sqrt{t/\tau_q} + ha} \tag{31}$$

This approximation, with the values in Table I, reproduces the two-variable function $Q_2(ha, t/\tau_q)$ with striking accuracy as exemplified in Fig. 4.

Since the numerical values of the parameters, α, β, and the A_i's, depend upon which t/τ_q interval the specific data point of interest belongs to (see Table I), several different sets of the parameters must generally be used to describe a decay curve. This is easy to implement on a computer. Some improvement of the approximation

Table III. Illustration of How the Final Results Depend on the Initial Parameter Estimates and on the Quencher Concentration in Single-Curve Analysis of 2D Quenching Data.[a]

Label	Conc. ($10^5 c_q$/Å^{-3})	Initial guess $\hat{ha}$	Initial guess $\hat{\tau}_q$	Final result ha	a	D	χ^2
				⟨1⟩	⟨13⟩	⟨5⟩	
3.1	0.5	0.5	50	1.35	8.4	8.94	1.036
		10	50	1.24	8.95	8.34	1.036
3.2	2.0	0.5	50	1.07	10.8	6.58	1.102
		20	20	∞	4.49	18.0	1.270
3.3	3.0	0.5	50	0.96	13.4	4.88	1.142
3.4	4.0	0.5	50	1.02	13.2	4.84	1.067
		2	20	1.01	12.7	5.18	1.070
				⟨10⟩	⟨13⟩	⟨5⟩	
3.5	1.0	2	50	14.9	12.3	5.48	1.116
3.6	4.0	2	50	11.4	12.9	5.07	0.841
				⟨∞⟩	⟨13⟩	⟨5⟩	
3.7	0.5	0.5	50	28.8	13.2	4.95	1.066
3.8	5.0	0.5	50	259	12.9	5.07	1.041

[a] The starting value of the third quenching parameter, a^3, was always 3000. The true parameter values are displayed in angular brackets. *ha* values greater than approx. 100 can be regarded as infinite and are therefore indistinguishable from each other.

Table IV. Illustration of How the Final Results Depend on the Quencher Concentration in Singe-Curve Analysis of 3D Quenching Data[a]

Label	Conc. ($10^5 c_q$/Å^{-3})	Final result ha	a	D	χ^2
		⟨1⟩	⟨13⟩	⟨5⟩	
4.1	0.5	0.75	13.7	5.60	0.956
4.2	3.0	0.94	13.2	5.14	0.884
4.3	5.0	1.01	12.8	5.04	1.120
		⟨10⟩	⟨13⟩	⟨5⟩	
4.4	1.0	17.2	12.3	5.14	1.118
4.5	5.0	8.70	13.4	4.86	1.184
4.6	12.0	9.69	13.0	5.06	1.106
		⟨∞⟩	⟨13⟩	⟨5⟩	
4.7	0.5	∞	12.6	5.21	1.072
4.8	5.0	∞	13.1	4.95	0.927
4.9	12.0	∞	12.9	5.09	1.204

[a] The true parameter values are displayed in angular brackets.

could have been achieved by using narrower t/τ_q intervals.

Figure 5 shows both $Q_2(ha, t/\tau_q)$ [Eq. (15)] for some values of *ha* and Owen's approximation [Eq. (19)] as functions of t/τ_q. Szabo's approximation [Eq. (20)] and our approximation [Eq. (31)] coincide almost perfectly with the displayed Q_2 data and are therefore not shown in the figure.

For the diffusion-controlled case the approximation becomes

$$Q^*_{2,\infty}(t/\tau_q) = A_1(t/\tau_q)^{\alpha} + A_2\sqrt{t/\tau_q} \qquad (32)$$

in some similarity with Eq. (19) but without exhibiting the unsatisfactory linear long-time behavior.

By differentiating Eq. (13) we find that the *relative* maximum error in F is dependent on the *absolute* maximum error in Q as

$$\left|\frac{\Delta F}{F}\right| = a^3 c_q |\Delta Q| \qquad (33)$$

Let us assume a value for the relative error in Q, $|\Delta Q/Q|$, and calculate Q, F, ΔQ, and ΔF from Eqs. (13) and (33) for a range of times [with reasonable values for $F(0)$, k_0, a, c_q, *ha*, and τ_q].

In Table II the values of ΔF thus obtained are compared to the statistical noise (given by $\sqrt{F}$) for some values of the relative error in Q. We observe that the

Table V. Illustration of How the Final Results Depend on the Initial Parameter Estimates and on the Quencher Concentration in Global Analysis of Diffusion-Influenced Fluorescence Quenching Data[a]

Label	Dimensions	Conc. ($10^5 c_q$/Å^{-3})	Initial guess $\widehat{ha}$	Initial guess $\widehat{\tau_q}$	Final result ha	Final result a	Final result D	χ^2
					⟨1⟩	⟨13⟩	⟨5⟩	
5.1	3D	1.2,2.0,3.0,5.0,8.0	0.5	50	0.98	12.9	5.11	0.965
5.2	2D	1.2,1.2,3.0,5.0	0.1	50	1.00	13.0	5.02	0.999
			1	50	1.01	14.4	4.21	1.005
5.3	2D	0.5,1.0,2.0,4.0	1	50	1.02	12.2	5.48	1.077
5.4	1D	1.0,2.0,4.0,6.0,7.0	2	100	0.97	13	5.07	1.017
					⟨10⟩	⟨13⟩	⟨5⟩	
5.5	3D	1.0,2.0,3.0,5.0	0.5	50	8.43	13.3	4.96	1.083
5.6	3D	0.5,1.0,2.0,3.0,5.0	20	20	12.7	12.6	5.12	1.047
5.7	2D	0.5,1.0,2.0,4.0	20	20	11.7	12.8	5.12	0.983
5.8	1D	1.0,2.0,4.0,5.0,8.0	20	20	9.73	13	5.02	1.036
					⟨∞⟩	⟨13⟩	⟨5⟩	
5.9	3D	2.0,3.0,5.0,8.0	10	10	∞	13.0	5.03	1.041
5.10	2D	0.5,1.0,2.0,3.0,5.0	100	100	∞	12.8	5.17	1.062
			20	20	99	13	5.03	1.061
				20	∞	12.8	5.14	1.061
5.11	1D	1.0,2.0,3.0,5.0,8.0	10	10	210	13	5.02	1.003
				10	∞	14.1	3.64	1.003

The starting value of the third quenching parameter, a^3, was always 3000 unless otherwise stated. The true parameter values are displayed in angular brackets. The underlined parameters were kept fixed in the analysis. *ha* values greater than approx. 100 can be regarded as infinite and are therefore indistinguishable from each other.

quality of the approximation is really an essential matter; if the deviation between true and predicted values is large (as for Owen's approximation for instance), the absolute error in F can be several times higher than the noise level, which is naturally a serious problem in the analysis. As evident from Fig. 4, the relative error for our Q_2 approximation is very small, in general less than 0.001, and is therefore not expected to cause any complications in the fitting of decay data.

Fluorescence Decay Data Analysis. Another difficulty in the analysis of diffusion data originates from the properties of the χ^2 hypersurface. For the sake of simplicity we omit the units of the fitting parameters in the following discussion. The units left out are as follows: for τ_q, nanoseconds (ns); for the interaction distance a, Ångströms (Å); for the diffusion coefficient D, Å^2/ns; and for the concentration c_q, Å^{-3} (number density), *ha* is dimensionless.

For all the decay data presented here, a fluorescence lifetime (τ_0) equal to 300 ns was used, since that lifetime is rather similar to the one for pyrene, which is often used as a fluorescence probe in quenching experiments. The rather long lifetime means that the time window monitored ranges from approx. 200 to 2000 ns, depending on the quenching efficiency and concentration. Other lifetimes have been tried and do not give rise to any unexpected deviations. The natural (unquenched) fluorescence lifetime should be determined in a separate experiment and should thereafter be kept fixed in the analysis.

In the early stages of the analysis of 2D data, we noticed that the parameter *ha* was usually easier to recover correctly than τ_q and a^3. We also found that keeping a^3 fixed in the analysis resulted in very good estimates of *ha* and τ_q, while keeping *ha* fixed did not much promote the recovery of the correct parameter values. Furthermore, we have observed that it is sometimes very difficult to find good initial guesses in the fitting of diffusion data.

All these observations can be readily explained from the cross sections of the χ^2 hypersurface, associated with 2D quenching, shown in Figs. 6–8, where the global minimum is located at $(ha,\tau_q,a^3) = (1,33.8,2197)$, thus corresponding to $a = 13$ Å and $D = 5$ Å^2/ns. The cross sections were cut by setting all parameters, except for the two under study, equal to their true values and then calculating the reduced χ^2 values for a large number of parameter combinations.

Table VI. Analysis of One-Dimensional Quenching Data with Two- and Three-Dimensional Models[a]

Label	Conc. ($10^5 c_q$/Å^{-3})	Model	Final result				
			ha	*a*	*D*	χ^2	χ^2_{1D}
			⟨1⟩	⟨13⟩	⟨5⟩		
6.1	1.0	2D	22.3	29.2	0.040	0.987	0.979
6.2		3D	87	49.3	0.006	0.977	
6.3	2.0	2D	23.4	31.2	0.032	0.999	0.979
6.4		3D	113	55.4	0.004	0.977	
6.5	7.0	2D	21.2	31.5	0.033	1.004	1.000
6.6		3D	74	47.9	0.006	0.986	
			⟨10⟩	⟨13⟩	⟨5⟩		
6.7	1.0	2D	∞	31.7	0.030	1.115	1.028
6.8		3D	∞	55.0	0.004	1.037	
6.9	4.0	2D	364	34.1	0.024	1.105	1.028
6.10		3D	∞	46.2	0.007	1.234	
			⟨∞⟩	⟨13⟩	⟨5⟩		
6.11	0.5	2D	∞	29.6	0.041	1.068	1.045
6.12		3D	∞	42.8	0.010	1.049	
6.13	5.0	2D	∞	35.3	0.021	1.003	1.002
6.14		3D	∞	48.8	0.006	1.123	
6.15	8.0	2D	∞	35.3	0.021	0.987	0.992
6.16		3D	∞	47.1	0.007	1.111	

[a] χ^2_{1D} represents the chi-square value obtained using the correct model. The true parameter values (corresponding to 1D quenching) are displayed in angular brackets.

In Figs. 6a and b the elongations of the χ^2 valleys in the τ_q and the a^3 directions, respectively, are evident. This implies that the parameter *ha* is determined much more precisely than τ_q and a^3, since for the latter two a wide range of values results in equally good χ^2 values.

Figure 6c shows a strong correlation between the parameters a^3 and τ_q. This is not surprising, since $\tau_q = a^2/D$, which means that an overestimated value of the diffusion coefficient can be compensated for by a smaller interaction distance. Figure 6c also gives the answer to why the fixing of *ha* does not help much in the recovery of τ_q and a^3, while, on the other hand, the fixing of a^3 makes the determination of τ_q quite unique.

Basically the same tendencies as in Fig. 6 can be observed in Fig. 7, where the χ^2 surface in the vicinity of the global minimum (at which $\chi^2 \simeq 1$) is displayed.

Figure 8 gives an overview of the surface $\chi^2 = f(ha, \tau_q)$, i.e., the same as in Figs. 6a and 7a. The broad valley in the *ha* direction is the key explanation for why it is sometimes very difficult to find good initial estimates in the fitting of diffusion data. By comparing Figs. 6a and 7a with 8, we notice that the huge valley in the *ha* direction is almost perpendicular to the small valley in the region near the global minimum. Therefore, a search from badly chosen initial guesses do not reach the interesting part of the χ^2 surface but may end up somewhere at the bottom of the large valley, in which χ^2 is almost *ha*-independent. However, if the initial guess is located in the very left part of the valley (*ha* less than approx. 10), where χ^2 is steadily decreasing toward the global minimum, the search will most likely be more successful. A further complication is that in the decay data analysis the third quenching parameter will generally be *unknown*, thus making the choice of starting values even more delicate.

From this we conclude that in the analysis of diffusion data it is crucial to examine the obtained results very critically and thoroughly investigate how the results are affected by different initial guesses. Without such tests the reliability of the results must be strongly questioned.

Single-Curve Analysis. Considering the problems outlined above, we have investigated the effect of the initial parameter estimates in conjunction with the quencher concentration on the final results. Some general observations concerning the analysis of diffusion-influenced fluorescence quenching data are presented.

Table VII. Analysis of Two-Dimensional Quenching Data with One- and Three-Dimensional Models[a]

Label	Conc. ($10^5 c_q$/Å^{-3})	Model	Final result			χ^2	χ^2_{2D}
			ha	*a*	*D*		
			⟨1⟩	⟨2⟩	⟨5⟩		
7.1	0.5	1D	(0.032, 107000)			1.344	1.036
7.2		3D	5.45	15.9	1.28	1.047	
7.3	4.0	1D	(0.068, 30000)			1.870	1.067
7.4		3D	2.73	22.2	0.98	1.062	
			⟨10⟩	⟨13⟩	⟨5⟩		
7.5	0.5	1D	(0.068, 46000)			2.163	0.948
7.6		3D	∞	20.5	0.989	1.044	
7.7	4.0	1D	(0.24, 7300)			7.139	0.841
7.8		3D	26.3	18.7	1.32	0.924	
7.9	6.0	1D	(0.36, 4200)			10.29	1.077
7.10		3D	26.8	18.2	1.40	1.118	
			⟨∞⟩	⟨13⟩	⟨5⟩		
7.11	0.5	1D	(0.073, 44000)			2.574	1.066
7.12		3D	∞	21.5	0.96	1.116	
7.13	5.0	1D	(0.41, 4000)			12.97	1.041
7.14		3D	191	18.8	1.32	1.056	

[a] χ^2_{2D} represents the chi-square value obtained using the correct model. The true parameter values (corresponding to 2D quenching) are displayed in angular brackets. For the 1D case, there are only two independent variables, namely, $K_1 = ha/\sqrt{\tau_q}$ and $K_2 = a^3/ha$. The resulting parameters K_1 and K_2 are displayed in parentheses. The true parameter values yield (K_1,K_2) values which are (0.172,2197) and (1.72,219.7) for $ha = 1$ and $ha = 10$, respectively.

It is important to be aware of the influence of the quencher concentration on the analysis. Especially for single-curve analysis it is crucial to use decay curves with a high enough quencher concentration in the fitting procedure. This is demonstrated for 2D data in Table III, where the starting-parameter dependence is also illustrated. The initial estimates can lead to false local minima, exemplified by the decay curve 3.2 with initial guesses $(\hat{ha}, \hat{\tau}_q, \hat{a}^3) = (20,20,3000)$. The $\chi^2 = 1.27$ is a bit higher than the best obtainable for that curve ($\chi^2 = 1.10$) but not high enough to call it a *poor* χ^2. However, the very low value of a, together with the high value of D, helps us to draw the conclusion that this is a false minimum. This procedure of rejecting the obtained results is of course not justified unless we can find a set of parameters which produces a lower χ^2 value.

It is fully possible to extract the desired quenching parameters from the analysis of a single decay curve, provided that the quencher concentration is sufficiently high. If "too low" a concentration is used, the results might be in great error as shown for curve 3.1. The curves with too low a concentration are often characterized by a high sensitivity to the starting parameters. At high quencher concentrations, the initial part of the decay curve becomes more predominant (higher curvature) than at low concentrations, in which case the decay is slow and (on a logarithmic scale) only slightly curved. This is so because at high quencher concentrations the $a^3 c_q Q_d$ term (nonlinear in time) is dominating over the $k_0 t$ term in Eq. (13).

Table IV presents the results of single-curve analysis of 3D data. The dependence on the initial estimates is much less pronounced in the 3D case than in the 2D, hence no starting values are shown in Table IV. From Tables III and IV is seems quite clear that it is more difficult to recover the true parameters for 2D data than for 3D data, thus implying a more shallow minimum in the χ^2 hypersurface. The general trend in the analysis of 1D, 2D, and 3D data is that the final results converge toward the true values as the quencher concentration is increased. In the 1D case, the fixing of the radius a makes the determination of the other two quenching pa-

Table VIII. Analysis of Three-Dimensional Quenching Data with a Two-Dimensional Model[a]

Label	Conc. ($10^5 c_q$/Å^{-3})	Model	Final result				
			ha	*a*	*D*	χ^2	χ^2_{3D}
			⟨1⟩	⟨13⟩	⟨5⟩		
8.1	0.5	2D	0.08	9.25	63.6	0.979	0.956
8.2	3.0		0.21	4.04	80.2	0.949	0.884
8.3	5.0		0.24	9.18	26.3	1.242	1.120
			⟨10⟩	⟨13⟩	⟨5⟩		
8.4	0.5		0.78	5.13	70.3	1.135	0.963
8.5	3.0		93.6	5.14	46.9	1.345	1.038
8.6	5.0		9.67	6.19	35.4	1.407	1.184
			⟨∞⟩	⟨13⟩	⟨5⟩		
8.7	0.5		1.19	5.24	69.6	1.403	1.072
8.8	5.0		∞	7.72	27.0	1.433	0.927
8.9	12.0		∞	8.70	20.8	1.511	1.204

[a] χ^2_{3D} represents the chi-square value obtained using the correct model. The true parameter values (corresponding to 3D quenching) are displayed in angular brackets.

Table IX. Illustration of How the Parameter Values Are Affected by the Use of an Incorrect Model in the Data Analysis[a]

Data	Model	χ^2	*ha*	*a*	*D*
1D	2D	OK	>20 times too large	≥2 times too large	100–200 times too small
1D	3D	OK, slightly higher than χ^2_{1D}	>100 times too large	1.5–10 times too large	20–1000 times too small
2D	3D	OK, slightly higher than χ^2_{2D}	2–3 times too large	~1.5 times too large	3–6 times too small
2D	1D	Poor, esp. for high values of *ha*	$ha\sqrt{D}/a$ more than 3 times too small a^3/ha more than 20 times too large		
3D	2D	$>\chi^2_{3D}$, poor for high values of *ha*	5–10 times too small	2–3 times too small	~10 times too large

[a] When using the 1D model in the analysis, there are only two independent parameters, $ha/\sqrt{\tau_q} = ha\sqrt{D}/a$ and a^3/ha, as discussed in the text.

rameters unique and is very insensitive to initial guesses. However, one should be aware that even rather small variations in the radius *a* can greatly affect the value of the diffusion coefficient *D*.

Global Analysis. We have tried to use global analysis [16] to reduce the sensitivity to the initial guesses, but the inherent problem with the flat valley in the χ^2 hypersurface partially remains. The global fitting of 2D and 3D data is rather insensitive to initial estimates and recovers the wanted parameters quite well (see Table V). Also, in global analysis one should pay attention to the effect of the quencher concentration on the results. The incorporation of low-concentration curves in the global analysis seems to make the search for the χ^2 minimum rather unwieldy and inefficient, since so many parameter combinations fit equally well to the low-concentration curves. This is demonstrated by comparison of the curve sets 5.5 and 5.6. The addition of a low-concentration curve to the data set 5.5 does not lead to better results, even though the χ^2 is decreased; on the contrary, the resulting parameters deviate even more from the true ones.

Distinguishing Between Different Dimensionalities. First, it should be made clear that a mere visual inspection of a fluorescence decay curve is not enough to determine which dimensionality it corresponds to. Our results

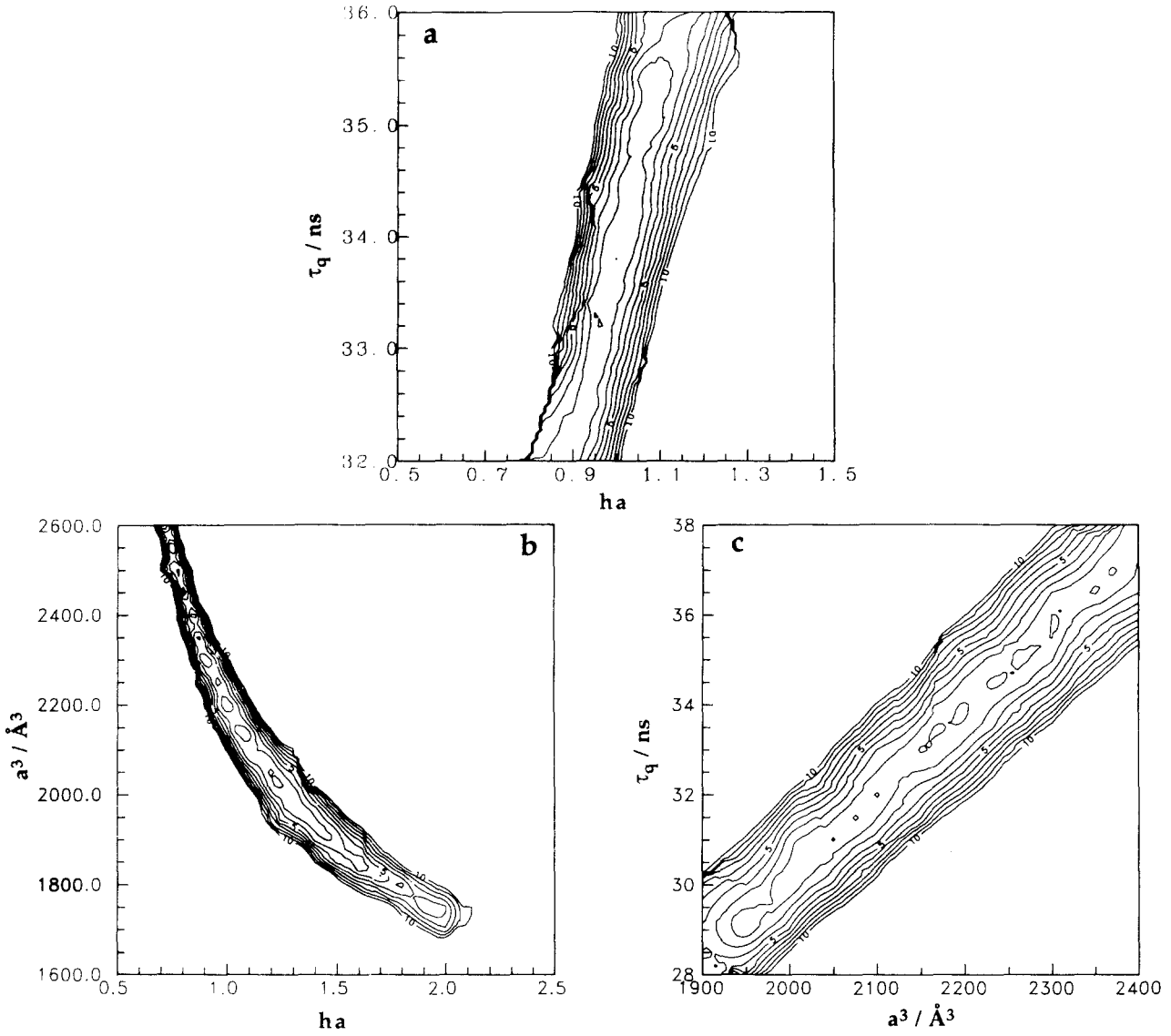

Fig. 7. The appearance of the contour plots displayed in Fig. 6, in the vicinity of the global minimum. Contour levels: $\chi^2 \leq 10$, $\Delta\chi^2 = 1$; (a) $\chi^2 = f(ha, \tau_q)$; (b) $\chi^2 = f(ha, a^3)$; (c) $\chi^2 = f(a^3, \tau_q)$.

indicate that data (in particular, not completely diffusion-controlled data) of a certain dimensionality can always be quite well described by a model of higher dimensionality; e.g., analysis of 1D data with 2D and 3D models produces χ^2 values, which are almost as good as the χ^2 for the true 1D model (see Tables VI and VII).

However, the reverse is not true; using a model of too low a dimensionality leads to χ^2 values which are significantly higher than the one for the correct model (see Tables VII and VIII). For purely diffusion-controlled data this behavior is very clear. From this we conclude that if a certain set of data fits equally well to all three models, then we are dealing with 1D data. If it can be described by 2D and 3D but not by 1D functions, then the data correspond to 2D quenching. The last alternative is obviously that the data can be described only by the 3D model.

Thus, by using this exclusion principle it is possible to distinguish between the different dimensionalities, but it should be noted that all three models have to be thoroughly tested in the analysis first. This reasoning is valid for ideal data; i.e., it is assumed that the only random error comes from the counting process. In the real experiment, however, a number of other processes (in addition to the statistical noise) may also distort the data, e.g., pulse pileup, rf pickup, background counts, timing

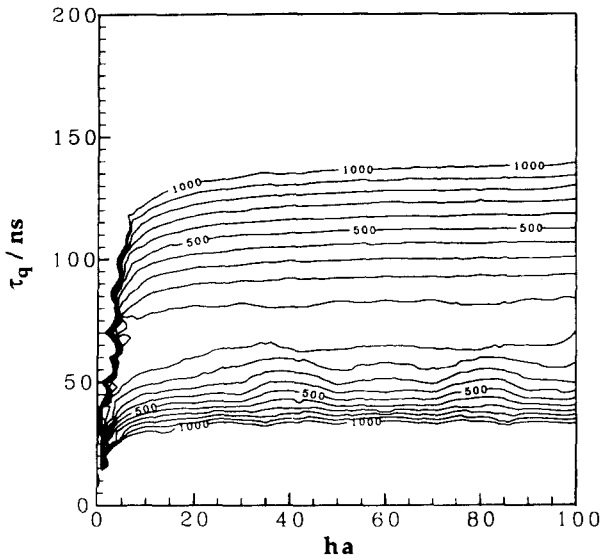

Fig. 8. Contour plot of the χ^2 cross section $\chi^2 = f(ha, \tau_q)$ for $\chi^2 \leq 1000$, $\Delta\chi^2 = 100$.

errors due to the limited performance of the electronics, etc. It could also be questioned, whether χ^2 is the best criterion for judging the goodness of a fit. Other statistical parameters, like the runs test or the Durbin–Watson parameter, do not necessarily lead to the same optimized parameters as the χ^2. It is therefore important not only to stick to the χ^2 values in the critical examination of the results obtained from fluorescence quenching data analysis. Even the actual parameter values have to be closely scrutinized. Physically unrealistic parameter values most likely indicate that the wrong model is used, even though the χ^2 value may be reasonably good. Using an incorrect model in the analysis, of course, results in erroneous parameter estimates. The general trends are summarized in Table IX.

CONCLUSIONS

In this work we have found that it is, at least in principle, possible to discriminate between different dimensionalities in fluorescence quenching experiments. In a forthcoming paper we will apply our findings to the analysis of real experimental data.

The designing of a fluorescence quenching experiment demands some comments.

The Probe. The choice of fluorescent probe is a critical matter, because the fluorescence lifetime sets an upper limit for the time interval that can be observed in the experiment. In order to study, for instance, 2D diffusion in a lipid membrane, the molecules must be allowed to diffuse for such a long time that the root mean square displacement is considerably larger than the membrane thickness; otherwise it is not meaningful to speak about two-dimensional diffusion, since it cannot be distinguished from three-dimensional. This point has, up to date, quite often been disregarded in the experimental studies of two-dimensional fluorescence quenching. For the same reason, also the fitting range has some effect on the results in the analysis of diffusion data; especially for slowly diffusing species, it is important to follow the diffusion process for as long time as possible.

The Quenchers. From our results we conclude that decay curves corresponding to high quencher concentrations should be preferentially used in the analysis of diffusion-influenced quenching data. However, the use of high-concentration samples is restricted by experimental factors; very high quencher concentrations might perturb structures and introduce new interactions in the system. The continuum model for diffusion should be questioned when the distance separating the quenchers becomes small, since the assumption that the motion of the quenchers is uncorrelated then might break down.

An increase in quencher concentration also leads to a shorter time window, which not only may necessitate the use of a time-consuming deconvolution procedure in the analysis, but also shortens the diffusive displacement during the measurements and, therefore, makes the 1D and 2D approximations bad, as discussed above.

The Decay Data Analysis. In the analysis of fluorescence decay data, a good χ^2 value, good-looking weighted residuals, and reasonable parameter values are not enough. It is also important to investigate the stability of the results obtained and to gain at least some information about the shape of the χ^2 hypersurface and the depth of the χ^2 minimum, for example, by trying multiple sets of initial guesses.

We can further note that *global* analysis does not lead to much better results than *single-curve* analysis; on the contrary, complications like the quencher-concentration dependence are more easily and quickly revealed by the latter. However, when the concentration influence is under control, then global analysis is more suitable, since it reduces the initial-value dependence. It should be emphasized that since all fitting parameters, except for the amplitudes, are common for a set of decay curves, the main feature of global fitting of diffusion data is to enable simultaneous analysis of the quenching behavior on different timescales.

As discussed above, the fixing of a is, in contrast to the fixing of ha, beneficial. This is fortunate, since a (corresponding to a radius or a layer thickness) can be

known or guessed with reasonable accuracy in many cases for hydrophobic membranes and rodlike micelles.

The method of creating an approximation to a multivariable function described in this paper should be a viable way also to treat other types of complicated functions, which otherwise would be practically unusable in fluorescence decay data analysis. This could be especially efficient in cases, where convolution effects also have to be taken into consideration; handling both Eq. (15) and numerical convolution is not realistic for analysis purposes, at least not with reasonable computation time. Equation (31), on the other hand, can be used in iterative reconvolution analysis without too much effort and CPU time consumption.

ACKNOWLEDGMENTS

Lars Ojamäe and Dr. Pehr-Åke Bergström, Institute of Chemistry, Uppsala University, are gratefully acknowledged for their kind assistance in the preparation of the contour plots.

REFERENCES

1. M. Smoluchowski (1917) *Z. Phys. Chem.* **92**, 129.
2. A. Szabo (1989) *J. Phys. Chem.* **93**, 6929.
3. F. C. Collins and G. E. Kimball (1949) *J. Colloid Sci.* **4**, 425.
4. M. Almgren, J. Alsins, E. Mukhtar, and J. van Stam (1988) *J. Phys. Chem.* **92**, 4479.
5. M. Almgren and J. Alsins (1991) *Israel J. Chem.* **31**, 159.
6. C. S. Owen (1975) *J. Phys. Chem.* **62**, 3204.
7. F. Caruso, F. Grieser, P. Thistlewaite, R. Urquhart, M. Almgren, and E. Wistus (1991) *J. Am. Chem. Soc.* **113**, 4838.
8. J. M. Vanderkooi, S. Fischkoff, M. Andrich, F. Podo, and C. S. Owen (1975) *J. Chem. Phys.* **63**, 3661.
9. K. Kano, H. Kawazumi, T. Ogawa, and J. Sunamoto (1981) *J. Phys. Chem.* **85**, 2204.
10. D. D. Miller and D. F. Evans (1989) *J. Phys. Chem.* **93**, 323.
11. M. Almgren and J. Alsins (1990) *Progr. Colloid Polym. Sci.* **81**, 9.
12. H. S. Carslaw and J. C. Jaeger (1959) *Conduction of Heat in Solids*, 2nd ed., Oxford University Press, New York.
13. K. R. Naqvi (1974) *Chem. Phys. Lett.* **28**, 280.
14. R. Das and N. Periasamy (1989) *Chem. Phys.* **136**, 361.
15. P. R. Bevington (1969) *Data Reduction and Error Analysis for the Physical Sciences*, McGraw–Hill, New York.
16. J. R. Knutson, J. M. Beecham, and L. Brand (1983) *Chem. Phys. Lett.* **102**, 501.